Observation of compressional Alfvén eigenmodes (CAE) in a conventional tokamak

W.W. Heidbrink[1]**, E.D. Fredrickson**[2]**, N.N. Gorelenkov**[2]**,
T.L. Rhodes**[3] **and M.A. Van Zeeland**[4]

[1] University of California, Irvine, USA

[2] Princeton Plasma Physics Laboratory, USA

[3] University of California, Los Angeles, USA

[4] Oak Ridge Institute of Science Education, Oak Ridge, TN, USA

Abstract
Fast-ion instabilities with frequencies somewhat below the ion cyclotron frequency occur frequently in spherical tokamaks such as the National Spherical Torus Experiment (NSTX). NSTX and the DIII-D tokamak are nearly ideal for fast-ion similarity experiments, having similar neutral beams, fast-ion to Alfvén speed v_f/v_A, fast-ion pressure, and shape of the plasma but with a factor of two difference in major radius. When DIII-D is operated at low field (0.6 T), compressional Alfvén eigenmode (CAE) instabilities appear that closely resemble the NSTX instabilities. In particular, the mode frequencies, polarization and beam-energy threshold are nearly identical to NSTX. CAE in high-field discharges and emission at cyclotron harmonics are also observed. As on NSTX, the basic stability properties are consistent with the idea that the instability is driven by anisotropy in the fast-ion velocity distribution and is damped predominantly by Landau damping of electrons. The results suggest that these modes might be excited in ITER.

(Some figures in this article are in colour only in the electronic version)

1. Introduction

Instabilities with frequencies $f = 0.4$–$1.1\ f_{ci}$ are observed in most beam-heated discharges in the National Spherical Torus Experiment (NSTX) [1]. (f_{ci} is the ion cyclotron frequency.) Similar instabilities were also measured in the mega ampere spherical tokamak (MAST) [2]. NSTX studies of the sub-cyclotron emission indicate that the instabilities are usually compressional Alfvén eigenmodes (CAE) [3–5], although some of the modes are probably global Alfvén eigenmodes [5]. The phenomenology of CAEs was studied extensively in NSTX [6].

In conventional tokamaks, fast-ion driven instabilities with frequencies at harmonics of the cyclotron frequency have been detected in numerous devices [7–18]; it has also been observed on a spherical tokamak [19]. This ion cyclotron emission (ICE) occurs under three conditions [20]: when beam ions are expelled to the plasma edge by instabilities, when finite-orbit effects create an anisotropic fast-ion population in the plasma edge, and at the onset of neutral beam injection when the distribution function is non-monotonic with energy.

Although ICE is often observed in conventional tokamaks, (to our knowledge) emission at $\sim 0.6 f_{ci}$ has never been reported. This raises the question: is sub-cyclotron emission peculiar to spherical tokamaks? Or can it occur in large-aspect ratio devices such as ITER?

The DIII-D tokamak and NSTX are nearly ideal for aspect-ratio studies of fast-ion instabilities [21]. Both devices use tangentially injected ~ 80 keV deuterium neutral beams to heat the plasma. DIII-D is able to approach the low toroidal field employed on NSTX, making it possible to match the most important dimensionless parameter for Alfvén mode stability, the ratio of fast-ion speed to Alfvén speed, v_f/v_A. The dimensionless fast-ion pressure, β_f, is also similar in the two devices. In addition, the cross-sectional shapes of the plasmas can be closely matched. Thus, it is possible to study Alfvén modes with all plasma parameters closely matched except the major radius, which differs by a factor of 2 in the two devices. The basic idea of the present study is to match NSTX conditions in DIII-D to see if CAEs are excited.

When DIII-D is operated at low toroidal field so that the injected beam ions are super-Alfvénic, instabilities with

the properties of the NSTX instabilities appear (section 2). Qualitatively, the observations agree well with CAE theory (section 3). Discrepancies with the theory (section 4) and the implications of the results for tokamak burning plasmas (section 5) are discussed in the final sections.

2. CAE measurements in DIII-D

After preliminary indications of CAE activity in a similarity study of toroidicity-induced Alfvén eigenmodes (TAEs) [21], the instrumentation was improved in preparation for the experiments reported here. The data in this paper consist of two parts. One set of data is from a 2004 experiment that was devoted to investigation of CAEs. The objective of this experiment was to replicate an earlier NSTX study [6]: an NSTX shape was selected and the neutral beam energy, injection angle and toroidal field were varied. The second set of data is from a variety of experiments that included low toroidal field operation during the 2005 campaign. These studies were directed towards other issues besides CAE stability. They span a wide range of plasma shapes, divertor configurations, plasma currents (0.3–1.4 MA) and toroidal fields (0.5–2.0 T).

In the dedicated experiment, deuterium, low-field (typically $B_T = 0.6$ T) DIII-D [22] plasmas are limited on the graphite inner wall and have a typical major radius of $R = 1.63$ m, minor radius of $a = 0.56$ m, elongation of $\kappa = 1.8$ and triangularity of $\delta = 0.46$ (figure 1). The temporal evolution of a typical discharge is shown in figure 2. As is typical in NSTX, beam injection commences during the current ramp. The maximum current of $I_p \simeq 0.61$ MA is large enough to minimize the beam–ion loss (prompt losses $\lesssim 10\%$) but small enough to avoid disruptions that occur when q_{95} approaches 3. (q_{95} is the safety factor at the surface that encloses 95% of the poloidal flux.) Early in the discharge, the q profile is probably reversed but eventually the current diffuses and sawteeth appear. Motional Stark effect measurements are unavailable in these low field discharges so the sawtooth inversion radius is used to constrain the EFIT equilibrium reconstructions [23].

The neutral beam injection energy ($E_{inj} = 45$–81 keV) and the injection angle are varied in nominally identical discharges. The so-called left beams have a tangency radius of $R_{tan} = 115$ cm, while the right beams have $R_{tan} = 76$ cm. The number of sources is adjusted when E_{inj} is changed to keep the injected power in the range of $P_B = 1.2$–2.5 MW. At these relatively modest power levels, the violent TAE activity and the consequent large fast-ion transport observed in previous low-field DIII-D experiments [15, 24] are avoided. Early in the discharge, modes with upward-sweeping frequencies in the 50–100 kHz range that are probably reversed shear Alfvén eigenmodes (also called Alfvén cascades) [25] are observed on magnetic and density interferometer diagnostics. Later in the discharge, modes with frequencies that coincide with the nominal TAE frequency are observed. These modes do not seem to have a strong impact on the CAE activity, however. The time evolution of CAE bursts differs from the time evolution of low-frequency fast-ion driven modes. Moreover, the measured neutron rate [26] is in excellent agreement with the classical predictions of the TRANSP simulation [27]
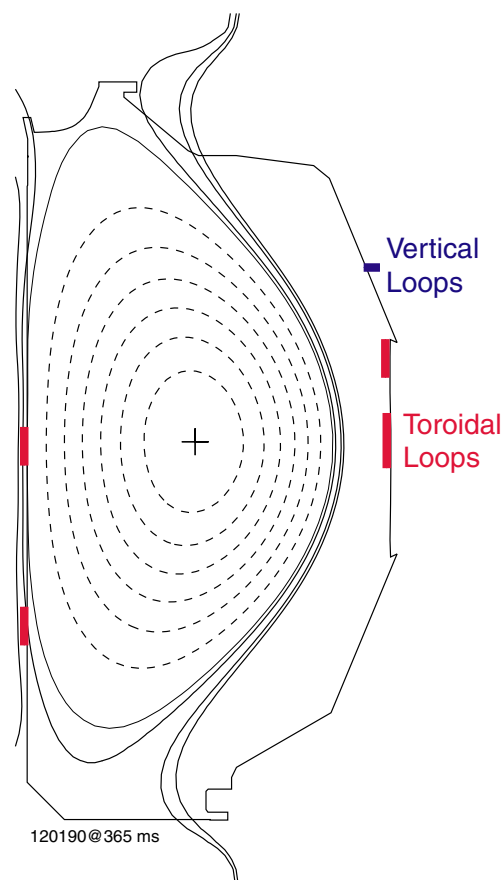

Figure 1. Equilibrium configuration in a typical discharge. The poloidal locations of the graphite tile loops and the vertical coils are indicated.

discussed in section 3, so any anomalous transport associated with the low-frequency AE activity is modest.

The plasmas undergo a transition to the H-mode, so the electron density n_e generally rises steadily during the first second of the discharge (figure 2(c)). Since the Alfvén speed is inversely proportional to $\sqrt{n_e}$ and the magnetic field and injection energy are constant, this implies that v_f/v_A also steadily increases as the discharge evolves.

CAE signals are detected by several diagnostics. Single-turn toroidal coils that use a modified plasma-facing graphite tile as a part of the conducting loop [28] measure $\dot{B}_\phi$ at several poloidal positions (figure 1). A set of vertical $\dot{B}_z$ coils that are mounted in a vacuum port at a ∼45° angle above the midplane also detect the CAEs; these coils have a bandwidth of ∼1 MHz. The CAE modes are also observed with a far-infrared scattering diagnostic that measures long wavelength ($k \simeq 1$ cm^{-1}) density fluctuations from most of the plasma volume. Density reflectometer diagnostics also detect CAE activity. The most sensitive CAE diagnostic is the toroidal loop on the outer midplane. (It also has the largest area of the toroidal loops.) Except where otherwise noted, all the fluctuation data in this paper are from this toroidal loop. Information on the spatial structure of the instabilities derived from the other diagnostics will be reported in a subsequent publication.
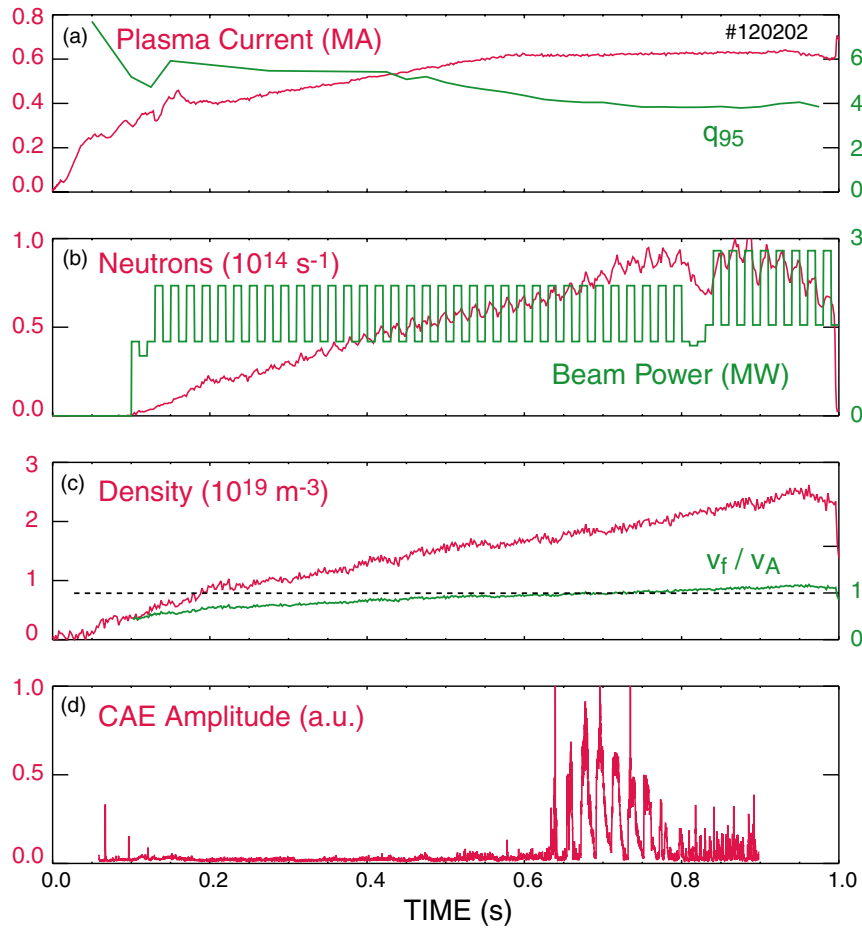
Figure 2. Time evolution of (*a*) the plasma current and the safety factor at the edge of the plasma, (*b*) the 2.5 MeV neutron rate and injected beam power, (*c*) the line-average density $\bar{n}_e$ and the ratio of the injected fast-ion velocity to the approximate Alfvén speed at $R = 210$ cm and (*d*) the amplitude of magnetic activity between 1 and 4 MHZ measured by the outer midplane graphite coil. The dashed line in (*c*) shows $v_f/v_A = 1$. $B_T = 0.6$ T; $E_{inj} = 55$ keV; left sources.

An example of the spectra measured with the graphite-tile loop is shown in figure 3. In this discharge, 80 keV left beams are injected half of the time. Bursts of modes with megahertz frequencies begin shortly after each beam pulse commences; the modes decay after each beam pulse on a millisecond timescale. The strongest activity occurs at ~2.5 MHz. The deuterium cyclotron frequency in this discharge is 4.5 MHz in the centre of the plasma and 3.6 MHz at $R = 210$ cm. (As discussed in the next section, the modes are probably excited in the vicinity of $R \simeq R_0 + 0.7a \simeq 210$ cm.) As in NSTX, many modes with different types of frequency spacings are seen. At the largest scale, bands of modes are separated by about 0.8 MHz. At the next scale, each band consists of several lines that are separated by about 110 kHz. At the finest scale, the lines often exhibit a fine splitting of ~20 kHz.

An example of CAE activity detected by the far-infrared scattering diagnostic is shown in figure 4. These measurements show that CAE modes cause density fluctuations in the plasma interior.

Figure 5 shows the plasma profiles at two different times for the same discharge shown in figure 3. At early times, the electron density is peaked on axis and is roughly parabolic in shape. After the transition to H-mode, the density rises and the profile of the electron density (and carbon impurity density)

exhibits a secondary lobe near the plasma edge. Although the activity is strongest when the density is low and the fast-ion pressure is large, clear signatures of CAE activity are detected throughout this discharge.

The frequencies of the instabilities correlate strongly with the toroidal field but more weakly with the electron density. The entire set of CAE measurements span a range in toroidal field from 0.5–2.0 T. Over this range, the observed frequency correlates strongly (correlation coefficient $r = 0.89$) with the Alfvén speed (figure 6). Since the cyclotron frequency also scales linearly with toroidal field, this indicates that the ratio of the mode frequency to cyclotron frequency f/f_{ci} remains approximately constant as the field varies. Figure 7(*a*) shows the time evolution of the activity in a dedicated discharge. The frequencies of the strongest modes decrease in time as the density rises but not as rapidly as the Alfvén speed, which varies as $\sqrt{1/n_e}$. Figure 7(*b*) investigates further the dependence of the mode frequency on density. The normalized mode frequency f/f_{ci} does correlate with density but the dependence is rather weak (correlation coefficient $r = -0.35$).

Rotation of the plasma can also influence the measured frequency. Toroidal rotation is expected to introduce a Doppler shift to the measured frequency of $\Delta f_{CAE} \simeq nf_\phi$, where n is the toroidal mode number of the CAE mode.
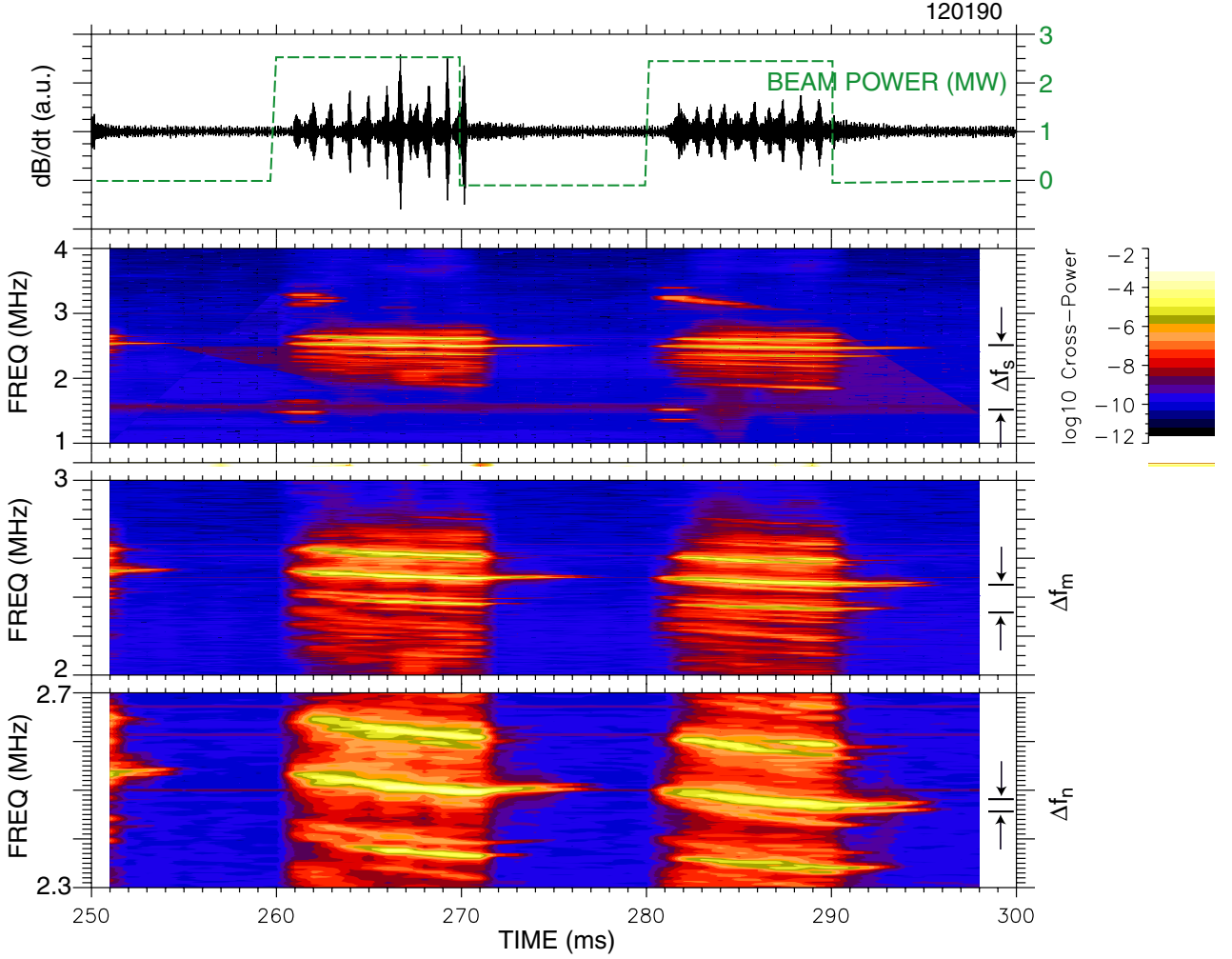
Figure 3. Time evolution of the magnetics signal and spectra in a discharge with periodic injection of 80 keV left beams. The spectra are shown in increasing detail to display the coarse (top), intermediate (middle) and fine (bottom) splitting. Reference [4] attributes this splitting to differences in radial mode number s, poloidal mode number m and toroidal mode number n. The bursts evident in the time series data do not appear in the spectra because a rolling 1 ms window is employed in the calculation of the fast Fourier transform. $B_T = 0.6$ T.

Charge-exchange recombination (CER) profiles of the toroidal rotation of carbon impurities [29] are available for most of the discharges. For the entire dataset, the normalized mode frequency f/f_{ci} correlates weakly with the toroidal rotation frequency (correlation coefficient $r = -0.26$). (Multiple regression indicates that this dependence is independent of the correlation with density.) The negative sign on the correlation coefficient indicates that the modes propagate opposite to the direction of beam injection and bulk plasma rotation. This is unusual: the shift for Mirnov modes and instabilities in the TAE frequency band is in the direction of the bulk rotation. It is also of interest to track the variation of the mode frequency as the discharge evolves. The usual 10 ms temporal resolution of the CER measurements is insufficient for these purposes but, in some instances, the rotation frequency can be inferred with $\sim$1 ms temporal resolution from Mirnov activity. Figure 8 compares the CAE spectra with the frequency of Mirnov activity during a portion of the discharge where v_A is nearly stationary ($\sim$2.6% variation in $\bar{n}_e$ during the interval shown in the figure). Some Mirnov and CAE frequency changes are correlated (e.g. at 782 ms) but others are not. In this

discharge, the Mirnov frequency increased $\Delta f_{\mathrm{Mirnov}} \simeq 1.8$ kHz between 751 and 782 ms, while the CAE frequency decreased $\Delta f_{\mathrm{CAE}} \simeq -43$ kHz. For a set of comparisons such as these drawn from twelve discharges with $\Delta v_A/v_A \lesssim 2\%$, the correlation between $\Delta f_{\mathrm{Mirnov}}$ and Δf_{CAE} is $r = -0.69$ and the inferred toroidal mode number is $n = -16 \pm 5$. Because the low-frequency $n = 2$ mode does not necessarily occur at the same radial location as the CAE mode (and because the CAEs probably have different toroidal mode numbers in different discharges), the large scatter in this comparison is not surprising. Nevertheless, the results clearly show that the CAEs rotate opposite to the direction of beam injection.

In plasmas with lower values of the injection energy during the dedicated experiment, the CAE activity often appears later in the discharge when the condition $v_f \gtrsim v_A$ is satisfied. This is clearly illustrated in the discharge with $E_{\mathrm{inj}} = 55$ keV shown in figure 2. Before 500 ms, any CAE activity is undetectable in the spectra. Beginning at 500 ms, weak activity is seen as v_f/v_A (evaluated at $R = 210$ cm) approaches unity. As v_f/v_A increases further, the activity grows stronger and multiple bands appear in the spectra. The strength of the activity is
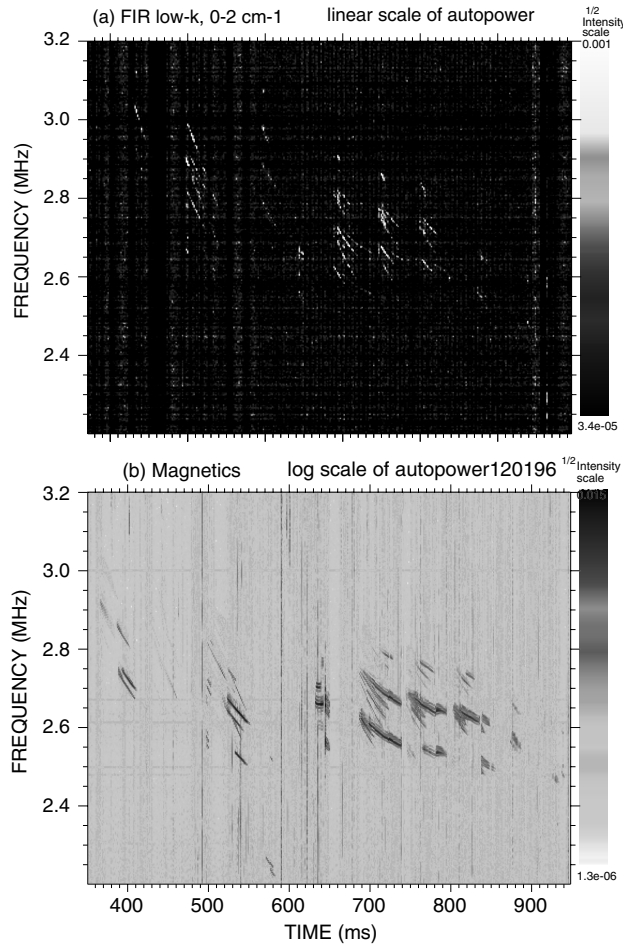
Figure 4. Spectra of (*a*) density and (*b*) $\dot{B}_\phi$ fluctuations in a 0.6 T discharge with the injection of 60 keV right beams.

clearly modulated at the same duty cycle as the beam power. After 800 ms, the activity weakens.

In general, CAE activity is readily observed when the beam ions are high energy and super-Alfvénic (figure 9(*a*)). As in NSTX, the beam injection energy must be $\gtrsim 50$ keV. Instability sometimes occurs with sub-Alfvénic fast ions but is less common. The most robust CAE activity occurs when $v_f \gtrsim 1.3 v_A$. Figure 9(*b*) shows the mode amplitude in four representative discharges from the dedicated experiment as a function of v_f and v_A (including the discharge shown in figure 2). The largest amplitudes occur for the largest values of v_f / v_A.

Nevertheless, CAE activity does occur in some high-field discharges with sub-Alfvénic beam ions. An example is shown in figure 10. CAE modes with $f = 5$–7 MHz appear both before and after the H-mode transition at 1.16 s. At any given time, only a single mode is excited. In the latter phase of the discharge, the mode is intermittent despite virtually constant plasma conditions. The single spectral line and variable excitation are common in plasmas that are near the stability threshold. In general, CAE activity at 2.0 T is only observed in plasmas with a relatively low electron temperature (figure 11). As discussed in section 3, the anisotropy in the fast-ion distribution function that drives the instability is strongest in plasmas with modest electron temperatures.

The dependence of CAE stability on plasma shape is weak. For the database, the stability properties are essentially uncorrelated with the size of the gap between the plasma surface and the inner or the outer wall. Instability correlates weakly with reduced plasma current, perhaps because the fast-ion banana width is larger at low current.

In some discharges, emission occurs above the cyclotron frequency. ICE occurs during plasma instabilities when sudden drops in neutron emission indicate that fast ions are expelled from the plasma. In discharges with modulated 80 keV beams, a ∼1 ms burst at harmonics of the central cyclotron frequency often occurs at the onset of each beam pulse, and then sub-harmonic emission ensues (figure 12). In discharges with steady lower voltage beams, the ICE often occurs early in the discharge when the electron temperature is very low ($\lesssim 0.3$ keV); then CAE activity with $f < f_{ci}$ prevails as T_e increases. Occasionally, both types of emission coexist for ∼25 ms as the instabilities transition between ICE and CAE activity. As shown in figure 13 for a database compiled from all the dedicated discharges, the electron temperature in the outer part of the plasma is nearly twice as large in plasmas with CAE activity than in plasmas with ICE (in plasmas with steady beam injection). As discussed below this trend is predicted by CAE theory.

3. Comparison with CAE theory

The excitation of compressional Alfvén waves by ion cyclotron resonances with energetic ions has been studied by many authors ([30] and references therein). The first to consider two-dimensional localization of the mode in both the radius and the poloidal angle was [30]. The theory was developed to explain ICE. To minimize Landau damping by electrons, the parallel phase velocity $\omega / k_\parallel$ was assumed to be large compared with the electron thermal speed. This condition often applies at the outer edge or the scrape-off-layer of the plasma, where the electrons are cold and ICE is excited by fusion products or ejected beam ions. In the case of ICE under steady-state conditions, the free energy that drives the instability is provided by anisotropy in the fast-ion distribution function. Both the fusion product birth profile and the neutral beam deposition profile normally peak strongly near the magnetic axis. Centrally-born, large-banana width, trapped fast ions can create a bump-on-tail velocity distribution that drives magneto-acoustic waves at the outer edge of the plasma.

After the observation of sub-harmonic emission in NSTX, it was recognized that, with minor modifications, the compressional eigenmode theory of [30] could also explain many features of the NSTX data [1, 3–5]. The key insight is that, in the NSTX case, the parallel wavenumber $k_\parallel$ is large (rather than small as in the ICE case). Large $k_\parallel$ has two implications. First, electron Landau damping is weak only if the electron thermal speed is fast compared with the parallel phase velocity, $v_e \gtrsim 3\omega / k_\parallel$. Second, the resonance condition for fast-ion interaction with the wave contains a large Doppler shift term $k_\parallel v_\parallel$, where $v_\parallel$ is the fast-ion parallel velocity. The resonance condition is

$$2\pi f = 2\pi f_{ci} - k_\theta v_{drift} - k_\parallel v_\parallel, \tag{1}$$

120190 @ 340 and 800 ms
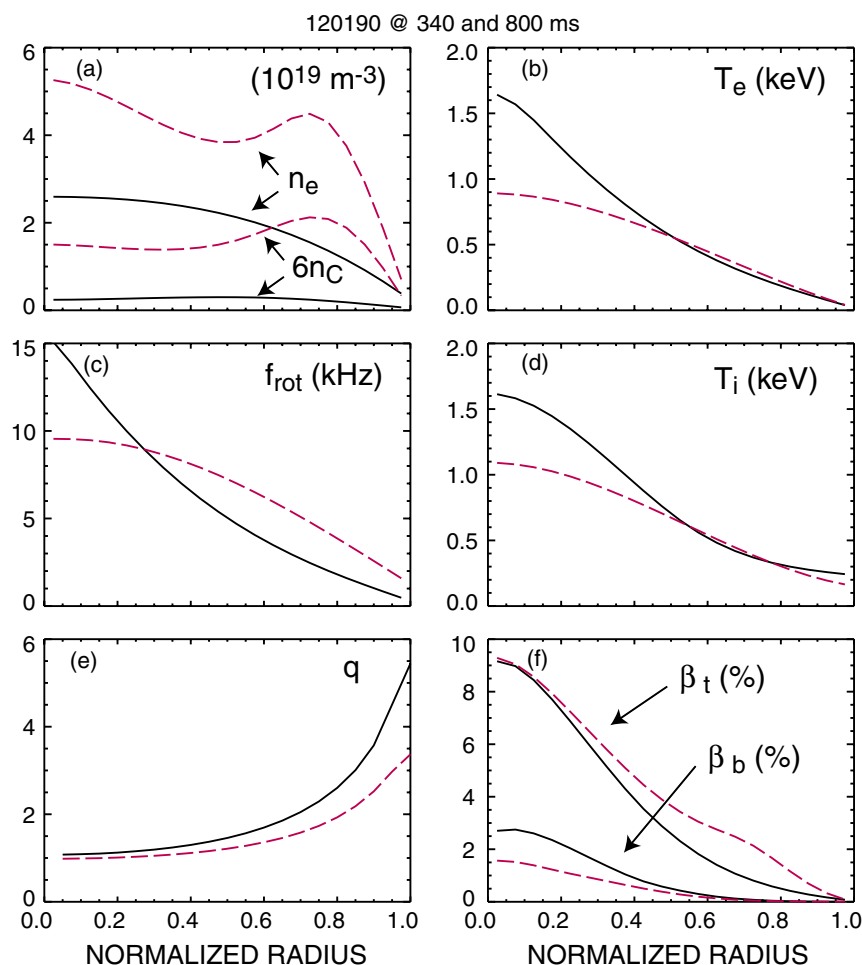
Figure 5. Radial profiles of (*a*) electron density from Thomson scattering [37] and interferometer [38] measurements, (*b*) electron temperature from Thomson scattering, (*a*) carbon density, (*c*) toroidal rotation frequency and (*d*) ion temperature from CER [29] measurements, (*e*) safety factor from EFIT reconstructions [23] that employ magnetics measurements and a constraint based on the soft x-ray inversion radius and (*f*) the total toroidal and beam betas as computed by TRANSP [27]. Times just before the first sawtooth (——) and after formation of the H-mode pedestal (- - - -) are shown.

where k_θ is the poloidal wavenumber and v_{drift} is the drift velocity. Since $k_\parallel v_\parallel$ is large, the mode frequency f is shifted significantly from the cyclotron frequency and damping on thermal ions is avoided. The free-energy that drives the instability is essentially the same as for the steady, edge-driven ICE: with central neutral beam deposition, the banana width of beam ions in NSTX is sufficiently large that the beam distribution develops a bump-on-tail velocity distribution in the outer portion of the plasma.

The DIII-D observations are in good agreement with all the main features of this theory. Although the polarization of the waves was not measured directly, the clearest signals are detected on the toroidal loops, which is consistent with the large toroidal magnetic field component that is expected for compressional Alfvén waves.

In CAE theory, the eigenmode is localized in a two-dimensional (radial and poloidal) potential well that is associated with spatial variations in the Alfvén speed. Figure 14 shows that a potential well exists for a DIII-D equilibrium with strong sub-harmonic emission. Recent calculations [31] with the NOVA-K code find radially and poloidally localized modes with frequencies that are
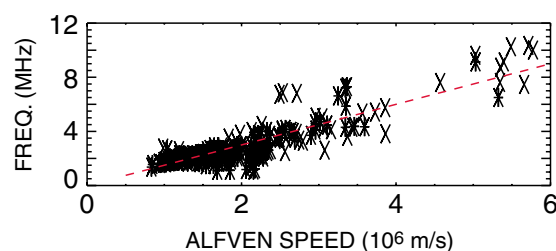
Figure 6. Frequency of the strongest mode with $1\,\text{MHz} < f < f_{\text{ci}}$ versus the Alfvén speed for all of the discharges in the database. The dashed line indicates a linear dependence on v_A.

consistent with the experimentally observed frequencies for DIII-D equilibria. These modes have the polarization of compressional waves. For numerical accuracy, the calculations assume $n = 0$ or $n = 1$ but it is likely that CAEs also exist theoretically for larger values of the toroidal mode number.

Unfortunately, it was not possible to accurately measure the toroidal mode numbers of the instabilities during this experiment, so the parallel wavenumber is uncertain.

329
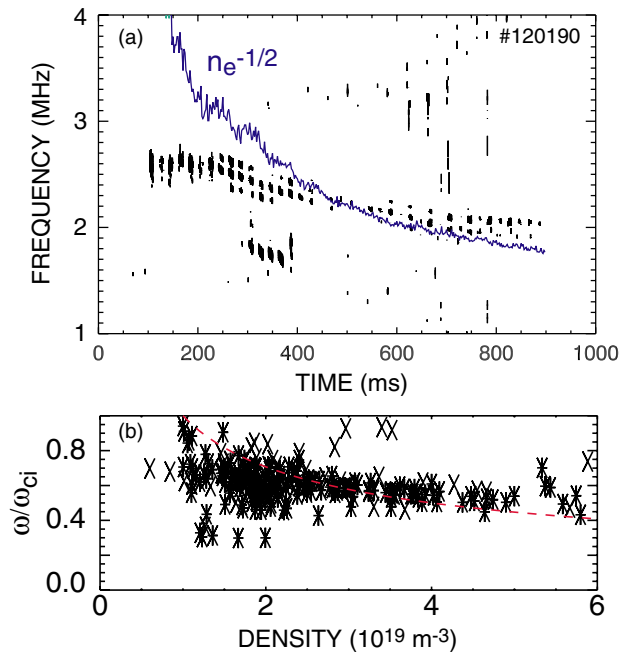
Figure 7. (*a*) Magnetics spectra for a 0.6 T discharge with periodic injection of 80 keV left beams. The temporal evolution of the Alfvén speed derived from an interferometer signal is also shown. (*b*) Normalized frequency of the strongest mode with $1\,\mathrm{MHz} < f < f_{ci}$ versus the line-average electron density for all the discharges in the database. The dashed line indicates a $n_e^{-1/2}$ dependence on mass density.

Inferences based on the observed Doppler shift suggest that the effective toroidal mode number is $n = O(-10)$ within large uncertainties. Nevertheless, it is possible to check the consistency of the observations with CAE theory for an assumed value of $k_{\parallel}$. First, reconsider figure 13. CAE theory predicts that $k_{\parallel}$ can either be small (for steady-state ICE) or large (for sub-harmonic emission) but that waves with intermediate values of $k_{\parallel}$ are too strongly damped to be unstable. Assuming that the CAE activity and the steady-state ICE are driven by the same population of fast ions, only the most unstable type of activity should appear. This is in qualitative agreement with the observation that sub-harmonic emission occurs in hotter plasmas, while steady-state ICE is seen in the coldest plasmas (figure 13). The electron Landau damping prediction is tested further in figure 15(*a*). For an assumed (but reasonable) value of $k_{\parallel}$, all the discharges with sub-harmonic modes lie at values of $\omega/(k_{\parallel}v_e) \lesssim 0.3$, while many of the stable discharges occur in plasmas where the electron Landau damping is large.

In calculations with an analytical distribution function, instability occurs when $k_{\perp}\rho_f$ exceeds unity [5]. Here $k_{\perp} \simeq \omega/v_A$ is the perpendicular wavenumber and ρ_f is the fast-ion gyroradius. The ordinate of figure 15(*a*) compares this theoretical prediction with the data. The observed threshold is of the correct order of magnitude but does not agree quantitatively with this prediction. The average value of $k_{\perp}\rho_f$ is 0.80 ± 0.25 for the unstable discharges and 0.55 ± 0.21 for the stable discharges. It seems likely that subtle details of the fast-ion distribution play an important role in driving the instability. In particular, the observed threshold in beam injection energy is rather sharp despite only a modest change in ρ_f.

Figure 15(*b*) examines the fast-ion resonance condition for all of the unstable discharges. For the same assumed value of $k_{\parallel}$ as in figure 15(*a*), the observed mode frequency is in rough agreement with the resonance condition but the correlation is weak (figure 15(*b*)). It seems likely that the actual value of $k_{\parallel}$ of the unstable modes differs significantly in the different plasma conditions. As expected, the Doppler shift is larger for the more tangential left sources than it is for the more perpendicular right sources. For the discharges in the dedicated experiment, the average frequency of the strongest CAE is $\langle f/f_{ci} \rangle = 0.56 \pm 0.07$ for the left sources and 0.69 ± 0.03 for the right sources.

To assess the availability of free energy to drive the modes, a TRANSP [27] calculation of the classical fast-ion distribution function is performed. Since the electron temperature (figure 5) of only ~ 1 keV in the low-field discharges implies a critical energy that is much less than the injection energy, the beam ions decelerate primarily on thermal electrons. Consequently, collisions with thermal ions are relatively weak and pitch-angle scattering events are rare, so the anisotropy of the injected fast-ion distribution function is preserved during thermalization. Figure 16(*a*) shows the calculated distribution function in the outer portion of the plasma. Two prominent 'ridges' of high density that are associated with ionization on the inside and the outside of the plasma, respectively, are apparent. Figure 16(*b*) shows representative orbits for fast ions in these high-density ridges. One orbit is a large banana-width trapped ion, while the other orbit is a strongly circulating passing ion. The trapped ions probably supply the free energy that drives the instability. As shown in figure 16(*a*), the resonance condition (equation 1) of the strongest observed mode passes through this bump in the distribution function.

In plasmas with higher electron temperature, collisions with ions become important and more pitch-angle scattering occurs prior to thermalization. The fast-ion population becomes more isotropic. This is the likely explanation for the observation that in the 2.0 T discharges CAE instability is more common in discharges with lower values of T_e (figure 11).

The polarization of megahertz modes was measured in NSTX [6]. For modes with the polarization of magneto-acoustic waves, the multiple frequencies in the spectrum never intersect as the discharge evolves. For GAE modes with the polarization of shear Alfvén waves, some of the lines in the spectrum merge and cross as the discharge evolves. In the DIII-D data, the spectral lines never cross, further supporting identification of these instabilities as CAE.

In summary, CAE theory successfully predicts all of the major trends in the data (table 1), confirming identification of these instabilities as CAEs. Discrepancies with the theory are discussed in the next section.

4. Discussion

In addition to explaining the broad features of the NSTX instability, [4] also proposes explanations for the various types of frequency splitting that are observed. The largest splitting is attributed to different radial mode numbers s within the potential well, the intermediate splitting is attributed to different poloidal mode numbers m and the fine splitting is

120196
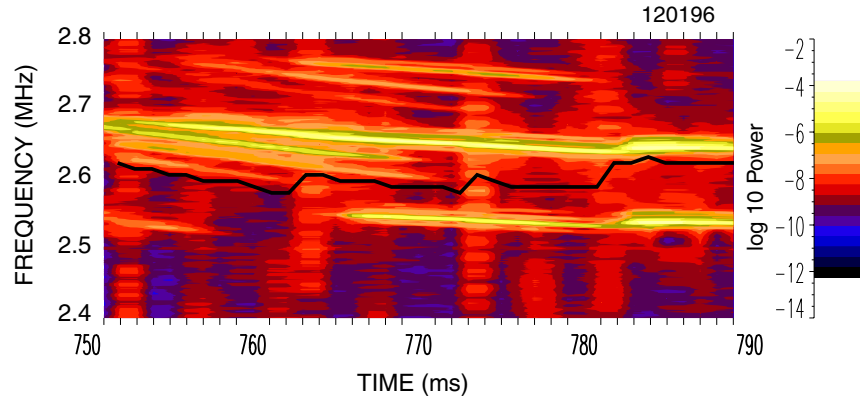
Figure 8. Magnetics spectra for a 0.6 T discharge with injection of 60 keV right beams. The thick solid line superimposes the temporal evolution of $\Delta f = n * f_{\rm rot}$, where $n = -16$ and $f_{\rm rot}$ is the measured frequency of a $\sim$9 kHz $n = 2$ Mirnov mode.
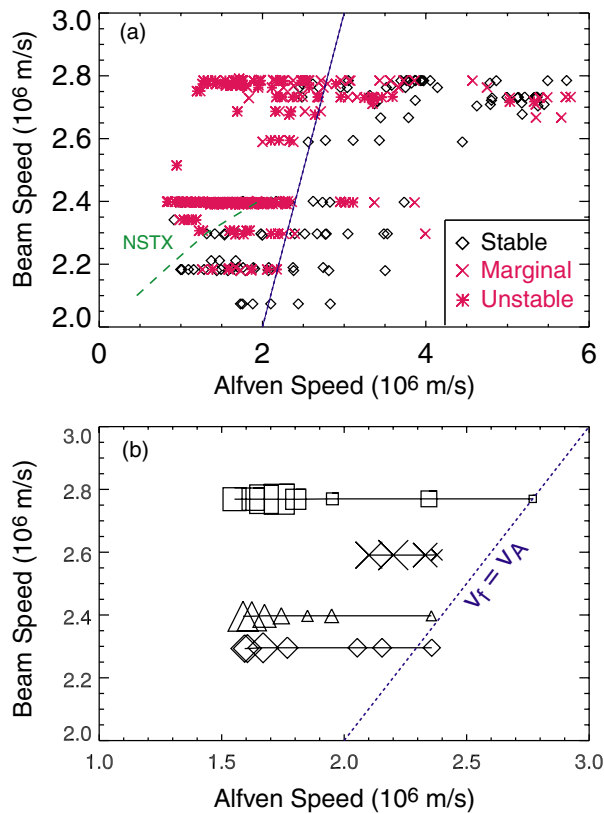

Figure 9. (*a*) Injected beam speed versus Alfvén speed evaluated near $R = 210$ cm for discharges with strong CAE activity ($*$), weak or intermittent CAE activity ($\times$) or no detectable modes ($\diamond$) for all the discharges in the database. The dotted line indicates equality between v_f and v_A. The empirical threshold in NSTX (from figure 6 of [6]) is indicated by the dashed line. (*b*) Data from four similar discharges with different values of $E_{\rm inj}$. The mode amplitude is indicated by the size of the symbol. The variation in v_A is due to evolution of the electron density.

attributed to different toroidal mode numbers n. Analytical estimates based on strong toroidicity theory find agreement to within $\sim$25% with NSTX measurements [4]. However, unpublished NSTX data suggest that this theory does not always fit the observations. Alternative theoretical expressions for the frequency splittings associated with the radial, poloidal and toroidal mode numbers are given in [32].
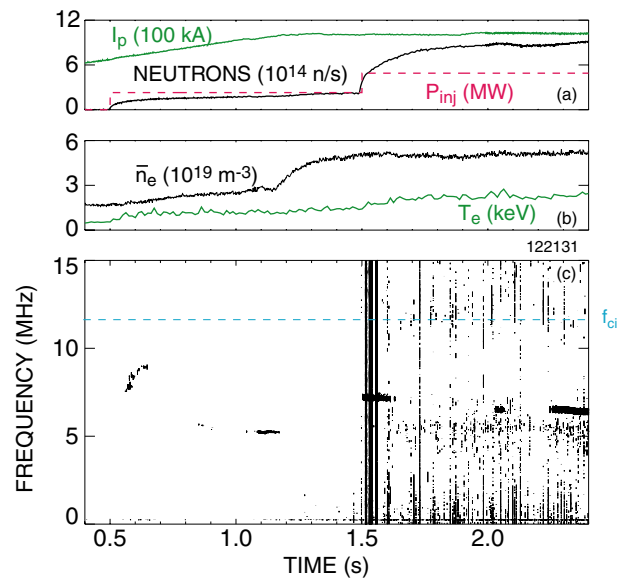

Figure 10. Time evolution of (*a*) the plasma current, neutron rate and injected beam power, (*b*) the line-average density $\bar{n}_e$ and central electron temperature and (*c*) spectrum of magnetic activity measured by the outer midplane graphite coil. The dashed line indicates the cyclotron frequency at $R = 210$ cm. $B_T = 2.0$ T; $E_{\rm inj} = 78$ keV; left sources.
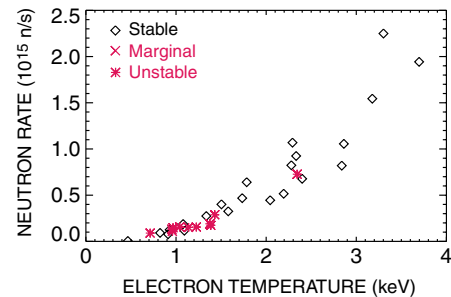

Figure 11. Neutron rate versus central electron temperature for all the discharges with $B_T > 1.9$ T in the database.

The coarse, intermediate and fine splitting patterns in DIII-D (figure 3) disagree with either of these analytical formulations [4, 32]. In particular, the observed splitting does not change as v_A changes, in contradiction to the predictions.
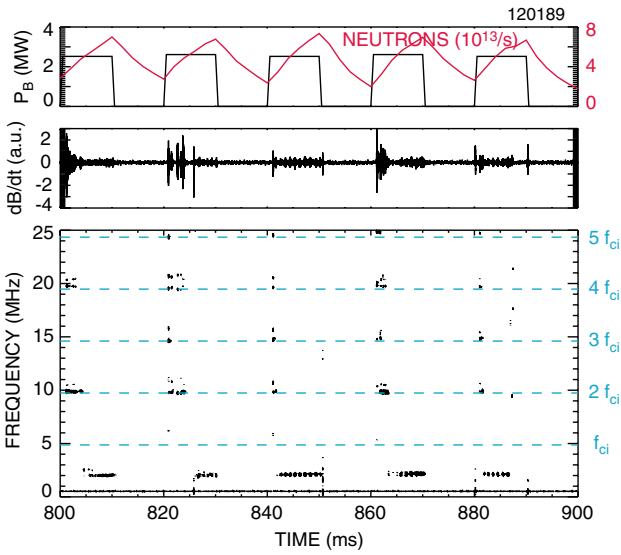
Figure 12. Injected beam power, 2.5 MeV neutron rate and $\dot{B}_\phi$ signal and spectra from the outer midplane graphite coil in a 0.6 T discharge with an injection of 80 keV left beams. Harmonics of the central ion cyclotron frequency are indicated by the dashed lines.
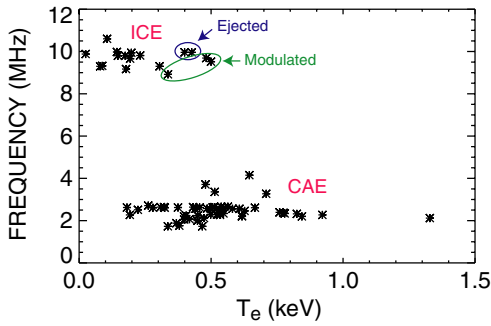

Figure 13. Frequency of the largest amplitude instability in the magnetics spectrum versus electron temperature at $R \simeq 210$ cm for all the discharges in the dedicated experiment. The points labelled 'Modulated' are from discharges similar to the one shown in figure 12 and the points labelled 'Ejected' are from a discharge with minor disruptions.

Evidently, alternative explanations for the peak splitting are needed. One possibility is that numerical calculations with actual equilibria are required. Another possibility is that toroidal rotation plays an important role. A third possibility is that the splitting has its origin in nonlinear effects. The spectral pattern will be examined in detail in a subsequent publication.

Instability is observed for smaller values of $k_\perp \rho_f$ than predicted by [4]. The typical value of $k_\perp \rho_f$ was higher in NSTX [6] but the difference between NSTX and DIII-D is probably a trivial operational one: NSTX experiments tend to operate at lower values of the magnetic field than DIII-D experiments. All indications are that the DIII-D plasmas become more unstable to CAE activity as B_T is reduced. Conversely, values of $k_\perp \rho_f$ below unity might be observed in NSTX if it were possible to operate the device at 0.6 T.

Recently, Belikov *et al* have suggested [33, 34] that the modes observed in NSTX are excited by a resonance with
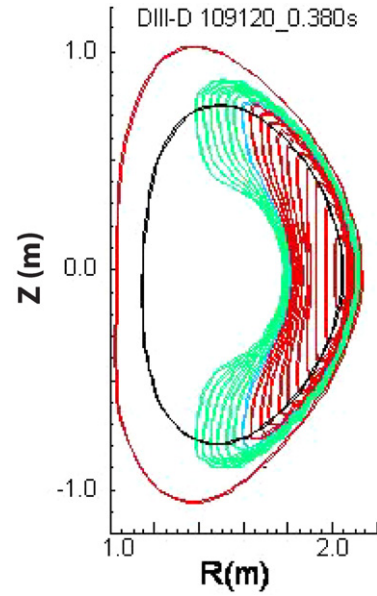
Figure 14. Approximate structure of the two-dimensional CAE potential well (linearly spaced contours) as calculated using the algorithm of [6]. A $n = 10$, $m = 1.5$ mode for the discharge of figures 1 and 5 is shown. The half-integer poloidal mode number means there are 1.5 wavelengths in the poloidal direction. (The wave is trapped poloidally, i.e. it forms a standing wave.)
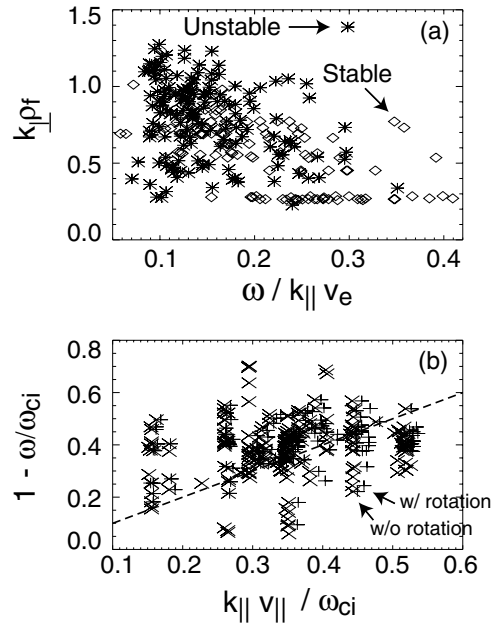
Figure 15. (*a*) $k_\perp \rho_f$ versus electron Landau damping parameter $\omega/(k_\parallel v_e)$ for all the discharges. $k_\perp$ is derived from the measured frequency (unstable points) or average measured frequency (stable points) and the Alfvén speed; ρ_f is from the cyclotron frequency, the beam injection energy and the nominal value of $v_\parallel/v$ for the left or right beam; all quantities are evaluated at $R = 210$ cm. (*b*) Comparison of the observed normalized Doppler shift $1 - f/f_{ci}$ with the expected Doppler shift $k_\parallel v_\parallel/\omega_{ci}$ for all the unstable points in the database. Perfect agreement with equation (1) is indicated by the dashed line. The + symbols include an approximate correction for the effect of bulk toroidal rotation on the observed frequency; the × symbols neglect this correction. Both figures assume $k_\parallel = 6.7$ m^{-1}.
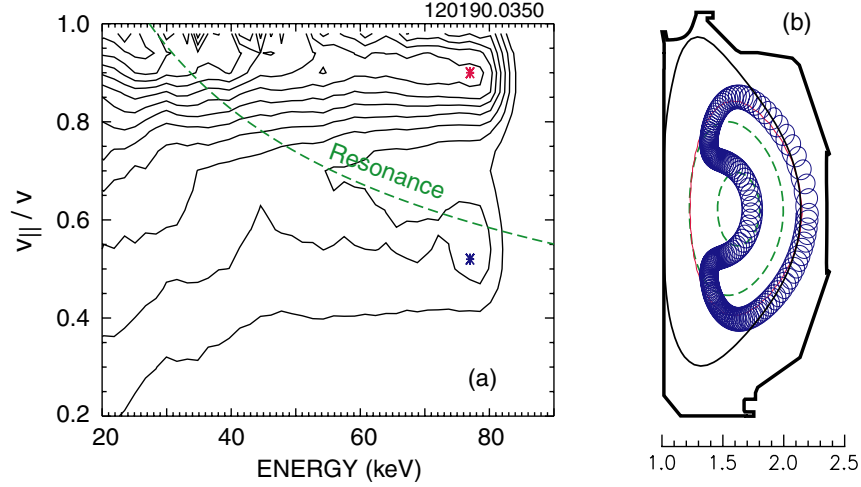
Figure 16. (*a*) Contours of constant fast-ion density near the outer midplane. The distribution function is calculated by TRANSP [27] for the radial profiles shown in figure 5, then is averaged spatially over the region bounded by normalized minor radii between 0.6 and 0.9 and poloidal angles of ±1 radian. The Doppler shifted resonance curve for the measured peak frequency and an assumed value of $k_\parallel = 7.5\,\text{m}^{-1}$ is indicated by the dotted line. (*b*) Projection of actual orbits for the two values of energy and $v_\parallel/v$ indicated by asterisks in the left-hand figure. The red orbit with the large pitch is strongly passing; the blue orbit with the lower pitch is a trapped orbit with large banana width.

circulating energetic ions,

$$2\pi f \simeq k_\parallel v_\parallel, \qquad (2)$$

rather than the resonance with trapped ions of equation (1). Equation (2) predicts that $k_\parallel$ is in the same toroidal direction as the beam injection, while equation (1) predicts that $k_\parallel$ is opposite to $v_\parallel$ of the beams. NSTX measurements with a toroidal array of magnetic coils [6] show that the mode propagation is anti-parallel to the injected beam ions, as predicted by equation (1). In DIII-D, the dependence of the mode frequency on the toroidal rotation velocity also indicates anti-parallel propagation.

Although CAE are readily excited by super-Alfvénic large-orbit fast ions, it should be noted that there is no evidence that the modes have a major impact on fast-ion confinement. Within experimental uncertainties of $\lesssim 15\%$ [26], the measured volume-average neutron rate during the dedicated experiment is in excellent agreement with the classically expected rate calculated by TRANSP. This agreement is in sharp contrast to the usual discrepancy when bursting instabilities in the TAE band of frequencies occur [35]. Presumably, the CAEs only impact the relatively small portion of the fast-ion population that resonates with the instability near $R = 210\,\text{cm}$. Similarly, in NSTX, the global implications of CAE activity on fast-ion confinement are probably minor [36].

5. Conclusion

Despite a factor of two difference in the aspect ratio, comparison of the instability in DIII-D with the NSTX phenomenology [6] shows that the instabilities are virtually identical.

- The mode frequency is $f \sim 0.6\,f_{\text{ci}}$.
- Three types of frequency splitting are observed.
- The mode has a large toroidal $\tilde{B}$ component.
- The phase velocity is less than the electron thermal velocity.

Table 1. Comparison of DIII-D data with NSTX [6] and the theory of [4].

Property	NSTX	DIII-D	Theory
Frequency	0.4–1.1 f_{ci}	0.3–1.1 f_{ci}	$\omega/\omega_{\text{ci}}$ $= 1 - k_\parallel v_\parallel$
Beam angle	$f \downarrow$ as $v_\parallel \uparrow$	$f \downarrow$ as $v_\parallel \uparrow$	$f \downarrow$ as $v_\parallel \uparrow$
Freq. evolution	$B/\sqrt{n_e}$	$\sim v_A$	v_A
Polarization	Compressional	$\tilde{B}_\phi$ large	Compressional
$k_\perp \rho_f$ Drive	$\gtrsim 1$	$\gtrsim 0.5$	1–2
Beam energy	$\gtrsim 60\,\text{keV}$	$\gtrsim 55\,\text{keV}$	$\rho_f, v_\parallel$
T_e dependence	—	$T_e \gtrsim 0.3\,\text{keV}$	$v_e \gtrsim 3\omega/k_\parallel$

- Instability occurs when the beam injection energy exceeds $\sim 55\,\text{keV}$.
- More modes and lower frequencies occur for injection angles with larger values of $v_\parallel$.

The instabilities in both devices are consistent with the broad features of CAE theory, confirming their identification as CAEs. In particular, the resonance condition is satisfied for reasonable values of $k_\parallel$, the electron damping is low for $v_e \gtrsim 3\omega/k_\parallel$, the predicted polarization is consistent with the observations, the dependence on injection angle ($v_\parallel$) is as expected and there is a non-monotonic feature in the velocity distribution. Future publications will compare the spatial structure of the mode and the frequency splitting with theory.

The observation of CAE instabilities in a conventional tokamak suggests that alpha particles may excite CAE instabilities in burning tokamak experiments. Figure 17 shows the distribution of alpha particles near the outer edge of a simulated ITER plasma. Because of finite orbit effects, the distribution function is anisotropic in this region. Since the electron temperature is high in the edge of ITER, electron Landau damping is easily avoided for reasonable values of $k_\parallel$, so alphas in the hump of the distribution readily satisfy the resonance condition (equation (1)). Moreover, the alphas in this hump have values of $k_\perp \rho_f$ (0.75) that are virtually identical to beam ions in DIII-D. Thus, it seems possible that CAE could

333
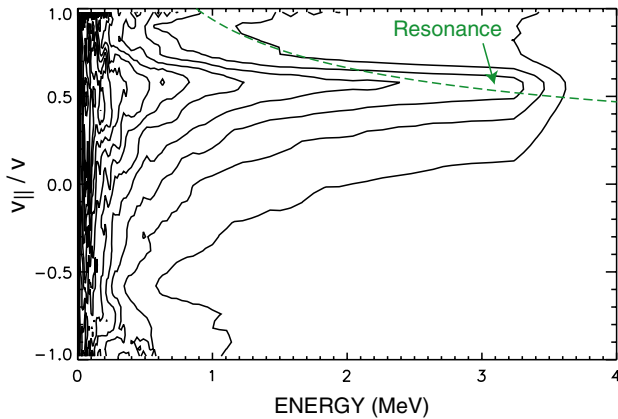
Figure 17. (*a*) Contours of constant alpha density near the outer midplane as calculated by TRANSP [27] for the ITER simulation described in [39]. The distribution function is averaged spatially over the region bounded by normalized minor radii between 0.9 and 1.0 and poloidal angles of ± 1 radian. The Doppler shifted resonance curve for an assumed frequency of $0.6 f_{c\alpha}$ (evaluated at the outer midplane) and the value of $k_{\parallel}$ that makes $\omega / k_{\parallel} = 0.3 v_e$ near the edge is indicated by the dotted line.

be excited in ITER. Theoretical stability studies are needed to investigate this possibility.

Acknowledgments

References

[1] Fredrickson E.D. *et al* 2001 *Phys. Rev. Lett.* **87** 145001
[2] Appel L.C., Akers R.J., Fülöp T., Martin R. and Pinfold T. 2004 Observation of CAEs on MAST *Proc. 31st European Physical Society Conf. on Controlled Fusion and Plasma Physics (London, UK, 2004)* p 4.195
[3] Gorelenkov N.N. and Cheng C.Z. 2002 *Nucl. Fusion* **42** 1216
[4] Gorelenkov N.N. *et al* 2002 *Nucl. Fusion* **42** 977
[5] Gorelenkov N.N. *et al* 2003 *Nucl. Fusion* **43** 228
[6] Fredrickson E.D., Gorelenkov N.N. and Menard J. 2004 *Phys. Plasmas* **11** 3653
[7] Equipe T.F.R 1978 *Nucl. Fusion* **18** 1271
[8] TFR Group 1983 *Nucl. Fusion* **23** 425
[9] Buchenauer D., Hwang D.Q., Mcguire K. and Goldston R.J. 1984 MHD effects on beam ion loss during near perpendicular neutral beam injection *Proc. 4th Int. Symp. on Heating in Toroidal Plasmas (Rome, 1984)* vol 1 p 111 (ISPP and ENEA)
[10] Yamamoto S. *et al* 1985 Plasma heating by multiple-short-pulse neutral beams *Plasma Physics and Controlled Nuclear Fusion Research 1984* vol 1 (Vienna: IAEA) pp 665–72
[11] Schild P., Cottrell G.A. and Dendy R.O. 1989 *Nucl. Fusion* **29** 834
[12] Seki M. *et al* 1989 *Phys. Rev. Lett.* **62** 1989
[13] Imai T. *et al* 1991 Lower hybrid current drive and higher harmonic ICRF heating experiments on JT-60 *Plasma Physics and Controlled Nuclear Fusion Research 1990* (Vienna: IAEA) vol 1 p 645
[14] Cottrell G.A. *et al* 1993 *Nucl. Fusion* **33** 1365
[15] Duong H.H. *et al* 1993 *Nucl. Fusion* **33** 749
[16] Cauffman S., Majeski R., Mcclements K.G. and Dendy R.O. 1995 *Nucl. Fusion* **35** 1597
[17] Mcclements K.G., Hunt C., Dendy R.O. and Cottrell G.A. 1999 *Phys. Rev. Lett.* **82** 2099
[18] Cottrell G.A. 2000 *Phys. Rev. Lett.* **84** 2397
[19] Mcclements K.G. *et al* 1999 *Plasma Phys. Control. Fusion* **41** 661
[20] Heidbrink W.W. And Sadler G.J. 1994 *Nucl. Fusion* **34** 535
[21] Heidbrink W.W. *et al* 2003 *Plasma Phys. Control. Fusion* **45** 983
[22] Luxon J.L. 2002 *Nucl. Fusion* **42** 614
[23] Lao L.L., St John H., Stambaugh R.D., Kellman A.G. and Pfeiffer W. 1985 *Nucl. Fusion* **25** 1611
[24] Heidbrink W.W., Strait E.J., Doyle E., Sager G. and Snider R.T. 1991 *Nucl. Fusion* **31** 1635
[25] Sharapov S.E. *et al* 2004 *Phys. Rev. Lett.* **93** 165001
[26] Heidbrink W.W., Taylor P.L. and Phillips J.A. 1997 *Rev. Sci. Instrum.* **68** 536
[27] Budny R.V. 1994 *Nucl. Fusion* **34** 1247
[28] Watson G.W. and Heidbrink W.W. 2003 *Rev. Sci. Instrum.* **74** 1605
[29] Gohil P., Burrell K.H., Groebner R.J. and Seraydarian R.P. 1990 *Rev. Sci. Instrum.* **61** 2949
[30] Gorelenkov N.N. And Cheng C.Z. 1995 *Nucl. Fusion* **35** 1743
[31] Gorelenkov N.N., Belova E., Fredrickson E. and Heidbrink W.W. 2006 *Nucl. Fusion* submitted
[32] Smith H., Fülöp T., Lisak M. and Anderson D. 2003 *Phys. Plasmas* **10** 1437
[33] Belikov V.S., Kolesnichenko Y.I. and White R.B. 2003 *Phys. Plasmas* **10** 4771
[34] Belikov V.S., Kolesnichenko Y.I. and White R.B. 2004 *Phys. Plasmas* **11** 5409
[35] Heidbrink W.W. *et al* 1999 *Phys. Plasmas* **6** 1147
[36] Fredrickson E.D. *et al* . 2002 *Phys. Plasmas* **9** 2069
[37] Carlstrom T.N. *et al* 1992 *Rev. Sci. Instrum.* **63** 4901
[38] Carlstrom T.N., Ahlgren D.R. and Crosbie *J. Rev. Sci. Instrum.* **59** 1063
[39] Budny R.V. 2002 *Nucl. Fusion* 1383